REGIONAL EVENT IDENTIFICATION RESEARCH IN ASIA

Hans E. Hartse, George E. Randall, Xiaoning (David) Yang, and Charlotte A. Rowe

Los Alamos National Laboratory

Sponsored by National Nuclear Security Administration
Office of Nonproliferation Research and Development
Office of Defense Nuclear Nonproliferation

Contract No. DE-AC52-06NA25396

ABSTRACT

Recent event identification efforts at Los Alamos National Laboratory (LANL) include mining event ground-truth data collection in central Asia, and efforts to improve the magnitude and distance amplitude correction (MDAC) discrimination methodology through derivation of Eurasian two-dimensional, regional-phase attenuation models and frequency-dependent Pn and Sn geometric-spreading models for a spherical Earth.

Our mining event efforts have identified mines around the former Soviet nuclear test site in eastern Kazakhstan. Using the Kazakh National Data Centre (KNDC) bulletin from 2002 to 2005, and waveforms recorded at station KURK and array MKAR, we combined time-of-day seismic event analysis, waveform cross correlations, seismic event location methods, image analysis, and seismic discrimination methods to identify active mines. Our goal was to tie event clusters with similar waveforms to specific mine sites, and thereby establish ground truth location and event type (earthquake or explosion) information. We found 13 event clusters that are probable mine sites, accounting for 277 individual seismic events. At least 4 of our event cluster locations are within 15 km of open pit mines, clearly visible on low-resolution imagery. All individual members of these clusters occur between 8am and 8pm local time. We presumed 75 local night-time events were earthquakes, and we found that none of these night time events had similar waveforms.

Using these probable mining events and the 75 unclustered night events as presumed earthquakes, we tested traditional body-wave discriminants in bands between 0.5 and 12 Hz, and find Lg spectral ratios and Pg/Lg high-frequency ratios show some ability to separate the event populations, but the separation is poor compared with the case of contained, single-charge explosions and earthquakes. The Pg spectral ratio, which has been shown to separate earthquakes and nuclear explosions in central Asia, does not separate mining explosions from earthquakes in eastern Kazakhstan. We will continue to investigate discriminant measurement and correction methods in an attempt to improve performance in separating mining events from both earthquakes and single-charge underground nuclear events.

In parallel with a project between the University of California, Santa Cruz (UCSC) and LANL to develop 1-Hz, two-dimensional, regional-phase attenuation models for Eurasia to improve the magnitude and distance amplitude correction (MDAC) discrimination methodology, we are working on developing regional-phase attenuation models for Eurasia for a broad range of frequencies between 0.5 and 10 Hz. We have finished an initial phase of data collection and amplitude measurement for around 100 stations in the region. Based on the data coverage, we collected a dataset of Pn picks from the LANL location database to be used in further data collection. We have also conducted synthetic simulations to investigate the geometric spreading of Pn and Sn in a spherical earth. From the modeling results, we propose new, frequency-dependent Pn and Sn geometric-spreading models for a spherical Earth.

While measuring phase and noise amplitudes using 20 sample per second (SPS) data obtained at Global Seismographic Network (GSN) stations operated through the Incorporated Research Institutions for Seismology (IRIS) International Deployment of Accelerometers (IDA) (II) group in Asia, we found that a combination of relatively early anti-alias filter roll-off and operations at relatively low gains, typically result in inaccurate registration of seismic noise and signals (from all but large events) in 6 to 8 Hz bands. Known II stations with this problem include AAK, BRVK, KURK, NIL, and TLY. This contrasts with other GSN stations in Asia where accurate 6 to 8 Hz measurements can be obtained from 20 SPS data streams.

OBJECTIVES

Over the past year we have continued studies to collect mining-event ground-truth data in central Asia, and we have continued efforts to derive Eurasian two-dimensional, regional-phase attenuation models and frequency-dependent Pn and Sn geometric-spreading models for a spherical Earth. The results of these efforts are all directed toward improved discrimination between earthquakes and explosions using regional and local seismic data.

RESEARCH ACCOMPLISHED

Kazakh Mining Ground Truth Study

We have been expanding our seismic ground truth data collection efforts for central Asia by identifying mines and mining explosion seismograms. Working with KNDC1 bulletins (2002–2005), we combine time-of-day seismic event analysis, waveform cross correlations, seismic event location methods, image analysis, and seismic discrimination methods to identify active mines in the area between International Monitoring System (IMS) array MKAR and Global Seismic Network (GSN) station KURK. Most of the events within this area occur during daytime (Figure 1), are usually small (often recorded at only one or two stations or arrays), and therefore tend to be poorly located. Our goal is to tie event clusters to specific mine sites, and thereby establish ground truth location and event type (earthquake or explosion) information.

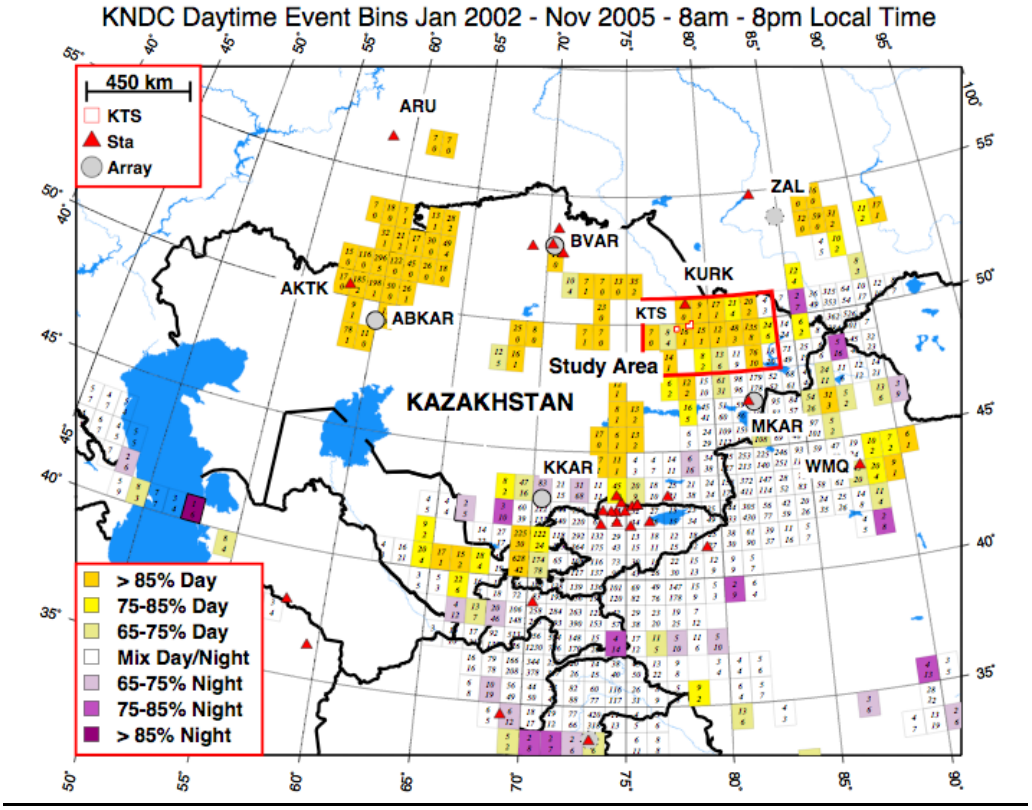

Figure 1. Time-of-day seismicity for Kazakhstan and surrounding regions. Primary event information source is the KNDC web-published bulletin. Gold and yellow regions are dominated by daytime mining explosions. Within each bin upper number is the daytime event count and the lower number is the nighttime event count. We focused on the area within the red box between array MKAR and station KURK in eastern Kazakhstan, which includes the former Soviet nuclear test site (KTS).

Using KNDC locations as a guide, we assembled about 450 three-component, event-segmented waveforms from MKAR array-element MK31. After bandpass filtering between 1.5 and 5.5 Hz, we then cross-correlated the first 20 seconds of each component's event-record with every other event record from the same component (that is, BHZ was correlated with other BHZ records, etc.). After stacking and normalizing the individual component correlations

into three-component correlations, we assembled similar-event clusters based on peak correlation coefficients exceeding 0.4. From the relative timing offsets within a given cluster's correlation peaks, we time-shifted, aligned, and stacked the individual event waveforms to create a single, three-component record at stations MK31 and KURK, and we stacked MKAR SHZ array elements. These waveform sums become the reference waves of each event cluster. Figure 2 shows the stacked BHZ wave and several aligned individual waves at station MK31 for event cluster A (see Figure 3 for event cluster locations).

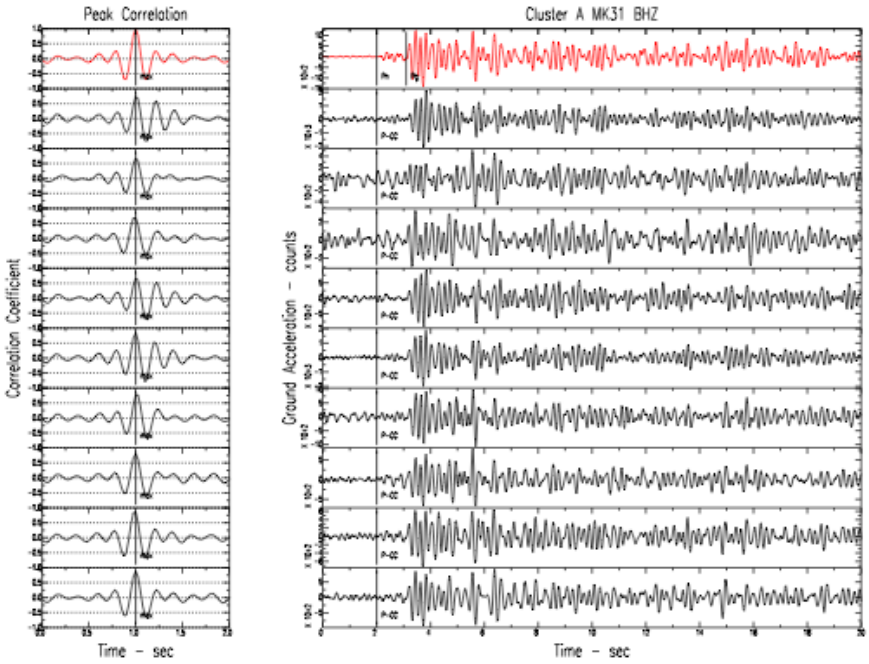

Figure 2. Event cluster A sample waveform stack (in red) and individual, vertical-component, time-aligned P-waves (in black) at MK31 BHZ. The three-component cross-correlation results are shown at left. Note improved signal-to-noise ratio on the stacked wave for Pn (first break). See Figure 3 for cluster locations.

We found 13 daytime clusters, each with 5 or more individual events, that are probable mine sites, accounting for 280 of the 450 KNDC events composing our original data set. We picked times of regional phases (Pn, Pg, Sn, and Lg) from each cluster's stacked waves at array MKAR and station KURK. We also estimated back-azimuths from MKAR by applying frequency wavenumber methods to the short-period, stacked array elements, and we estimated back-azimuths from the stacked, three-component waves at KURK when signal-to-noise was favorable. Using the picks and back-azimuth estimates we re-located each mining-event cluster, thus reducing the 280 individual KNDC locations to 13 cluster locations (Figure 3). Event-station distances for the clusters are between about 75 and 550 km and most individual event magnitudes are between about 1.25 and 2.5 mb.

We found that nearly every clustered event occurred between hours 02 and 14 GMT, or between 8 am and 8 pm local time (Figure 4). We assume the unclustered night events are earthquakes (solid blue circles, Figure 3), and thus have been able to test body-wave discriminants following standard processing methods outlined in Hartse et al. (1997). The Pg/Lg high-frequency discriminant shows some event separation (Figure 5), but not the separation seen between earthquakes and single-charge, contained explosions (Hartse et al., 1997). The Lg spectral ratio does not appear to separate the mining explosions from the earthquakes (Figure 5). We will continue to investigate discriminant measurement and correction methods in an attempt to improve performance in separating mining events from earthquakes and from single-charge, contained explosions.

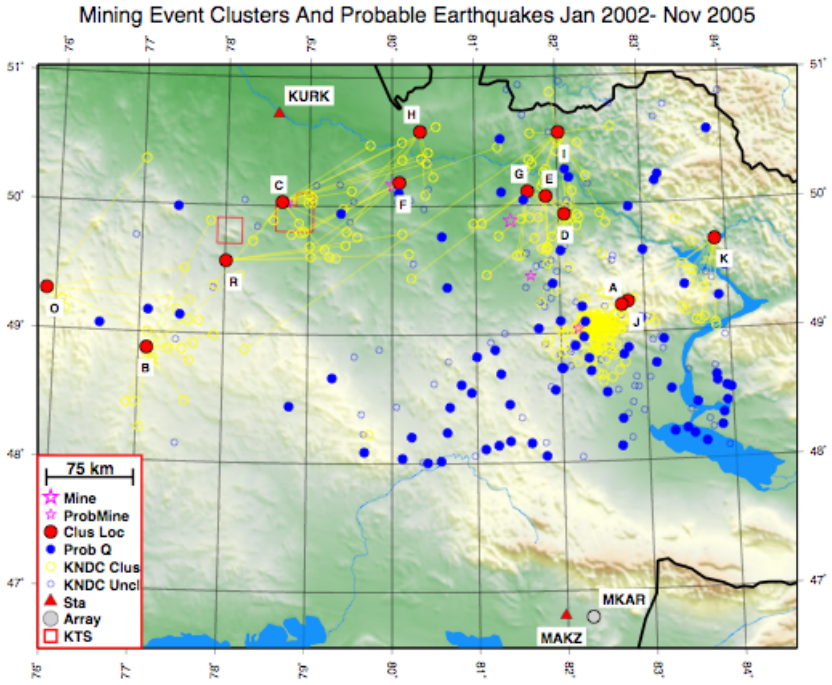

Figure 3. Study area showing individual KNDC locations (open yellow circles), which we formed into 13 event clusters (follow yellow lines to solid red circles). Solid blue circles show presumed earthquakes (unclustered night events), and open blue circles are remaining unclustered day events, which could be earthquakes or explosions.

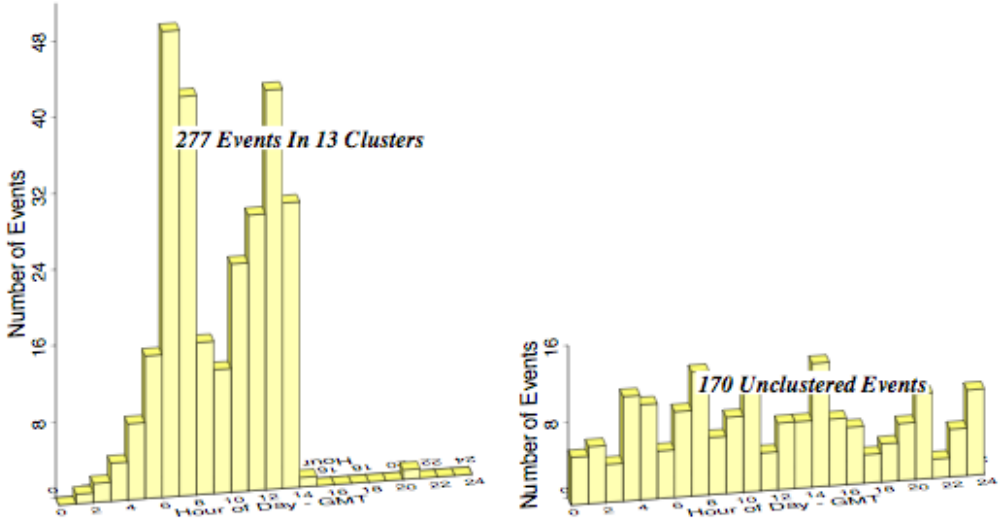

Figure 4. Time-of-day histograms for seismic events in study area. Left shows events associated with the 13 clusters. Local noon is 6 GMT. Note nearly all event activity abruptly ends at 1400 GMT, or 8 pm local time, another indication of mining activity. Histogram on right shows the 170 unclustered seismic events from within the study area. Only slightly more events are occurring during local day compared with local night, suggesting most day-time mining events have been successfully clustered.

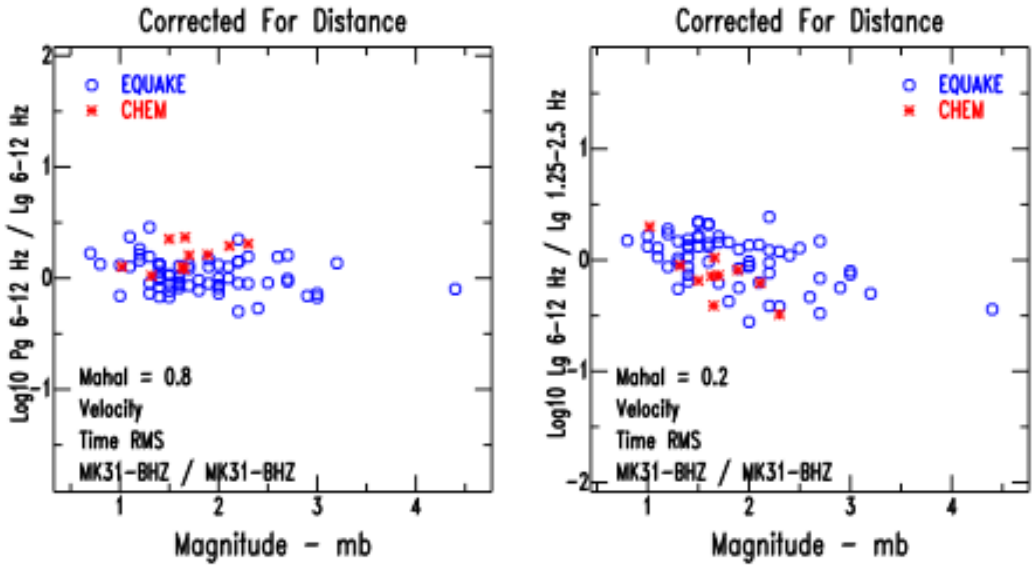

Figure 5. Sample discriminants. Only simple distance corrections have been applied. The high-frequency Pg/Lg shows some separation (left). The Lg spectral ratio shows little separation (right).

Based on seismic locations we have identified some mines on Google Earth and other images (Figure 6). Despite using only two stations at distances of up to 550 km, we have found at least four mine images that are within 14 km of our seismic locations. Improved seismic locations will allow for better ties between the seismicity and the mines in this area.

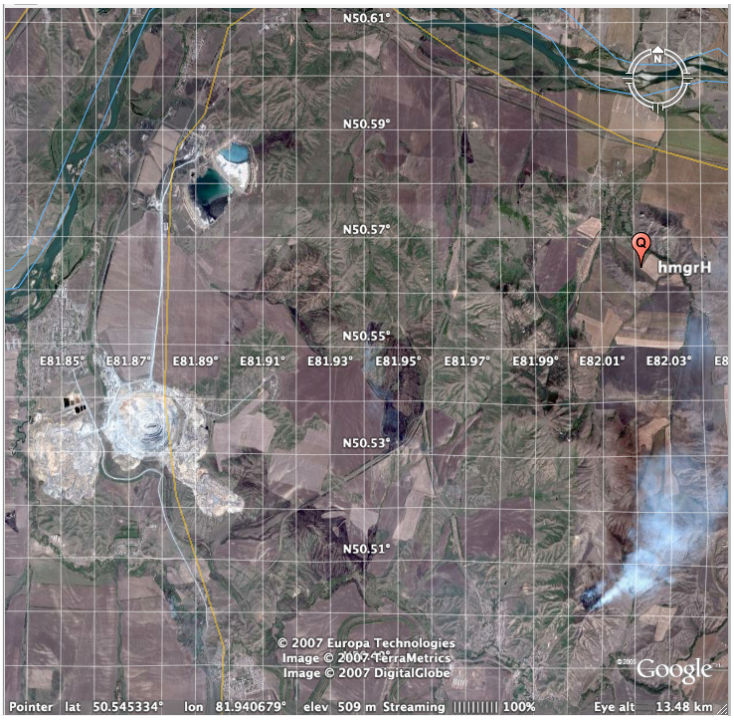

Figure 6. Google Earth image showing open-pit mine (on left) and seismic location of event cluster H with label "hmgrH" (on right). Separation distance between mine and seismic location is about 12 km.

Pn Attenuation Tomography between 0.5 and 8 Hz and Development of a New Pn Geometric-Spreading Model

Two-dimensional regional-phase (Pn, Pg, Sn and Lg) attenuation models improve the performance of MDAC methodology by providing better path corrections. Since regional-phase amplitudes in different frequency bands are used in MDAC corrections to form discriminants, regional-phase attenuation models for corresponding bands are needed. One method of obtaining the models at different frequencies is to derive the model at 1 Hz and use an assumed relationship between frequency and attenuation coefficient to deduct attenuation models at other frequencies. A second approach is to develop attenuation models at multiple frequency bands directly from observed data. Based on the second approach, we are developing regional-phase attenuation models for Eurasia for a broad range of frequencies between 0.5 and 8 Hz. Our focus has been on developing Pn attenuation models. This effort is in parallel to a project between UCSC and LANL to develop 1-Hz, 2D regional-phase attenuation models for the same region (Lay, et al., 2006).

We have finished two rounds of data collection and amplitude measurement. We collected waveform data from the Data Management Center (DMC) of the IRIS and from the LANL GNEMRE database. Using these waveform data, we made regional-phase amplitude measurements at frequencies of 0.5, 0.75, 1.0, 1.25, 1.5, 2.0, 2.5, 3.0, 4.0, 6.0, and 8.0 Hz. We used a semi-automatic procedure based on analyst picks and/or nominal regional-phase travel times to window different phases for amplitude measurement. Figure 7 shows the path coverage of 1-Hz Pn amplitudes that have signal-to-noise ratio of 2 or larger and a source-receiver distance of 2,000 km or shorter. We are currently collecting more amplitude data based on Pn picks stored in the LANL GNEMRE location database in order to improve coverage in certain areas. Figure 8 shows the path coverage of Pn picks from the database. Using this dataset, we hope to improve Pn path coverage, especially in northern Eurasia and India to some extent.

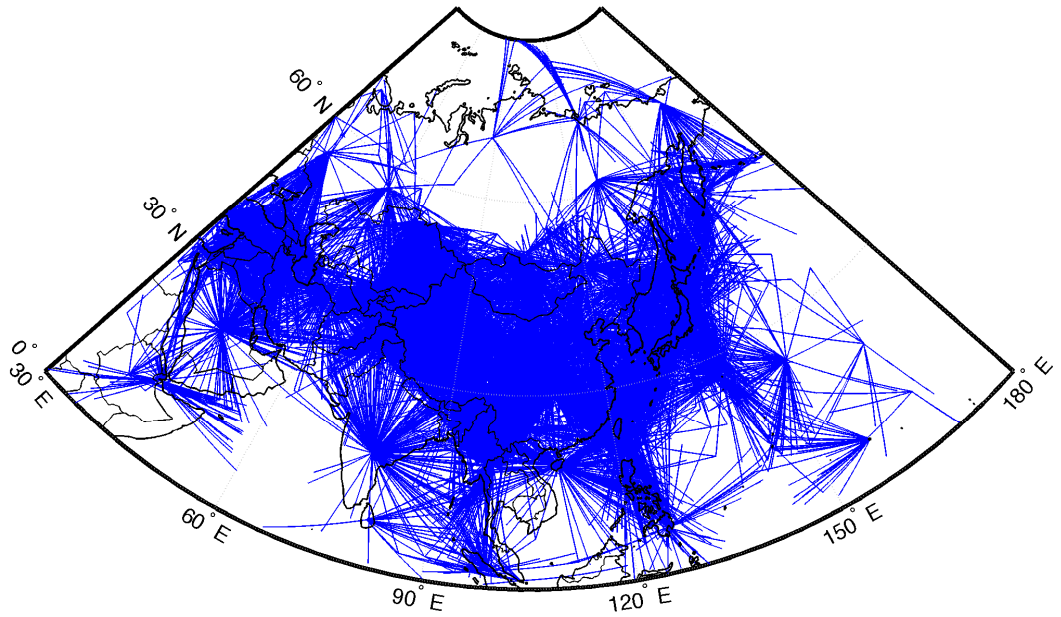

Figure 7. Path coverage of 1-Hz Pn amplitude measurements with signal-to-noise rates of 2 or larger and path lengths of 2,000 km or less.

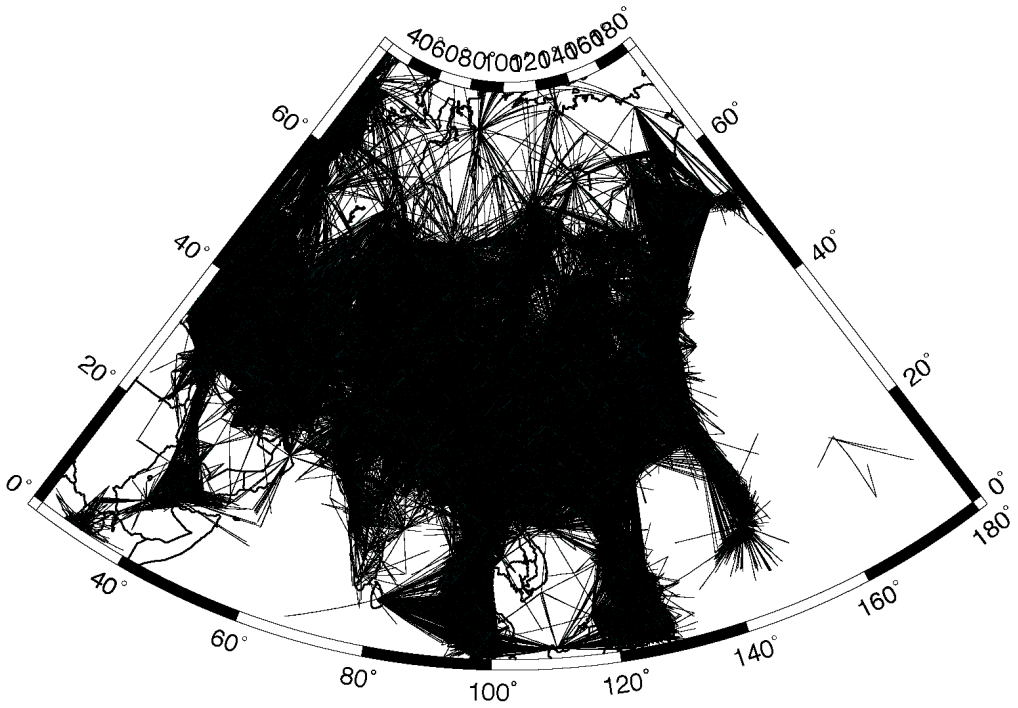

Figure 8. Path coverage Pn picks from the LANL GNEMRE location database.

Because of the tradeoff between geometric spreading and attenuation, it is necessary to accurately constrain the geometric spreading of the regional phases in order to develop reliable regional-phase attenuation models. Whereas the geometric spreading of crustal phases Pg and Lg may be relatively simple (Yang, 2002), the geometric spreading of upper-mantle phases Pn and Sn is more complex due to the sensitivity of these phases to the upper-mantle velocity structure and the Earth's sphericity.

In collaboration with researchers at UCSC, we conducted detailed simulation of Pn geometric spreading in a spherical Earth model. In order to quantify the first-order effects of the Earth's sphericity on Pn geometric spreading, we used a simple one-layer-crust over a constant-velocity-mantle spherical elastic Earth model in our simulations. We specified a crustal thickness of 40 km, representative of continental crusts. A reflectivity method was used to calculate synthetic Pn seismograms after the spherical Earth model was transformed into a plane-layered model through the Earth flattening transformation.

Figure 9 gives an illustration of Pn propagation in a spherical Earth from the simulation. On the left is the record section of synthetic Pn seismograms. Pn amplitudes as a function of epicentral distance and frequency are plotted on the right. The figure reveals several interesting characteristics of Pn traveling in a spherical Earth. Due to the Earth's sphericity, the apparent Pn velocity is not constant, but varies with epicentral distance. As is predicted by theory (e.g., Červený and Ravindra, 1971), the pulse shape of Pn evolves from that of the source, which is an impulse, at distances close to the critical distance (about 0.8°) to the shape of a far-field body wave, which is the time derivative of the source pulse, at farther distances. At about 10° to 12°, the wave that has no reflection at the Moho separates from the rest of the Pn wave packet and, somewhere between 16° and 19°, the wave that reflected once at the Moho separates.

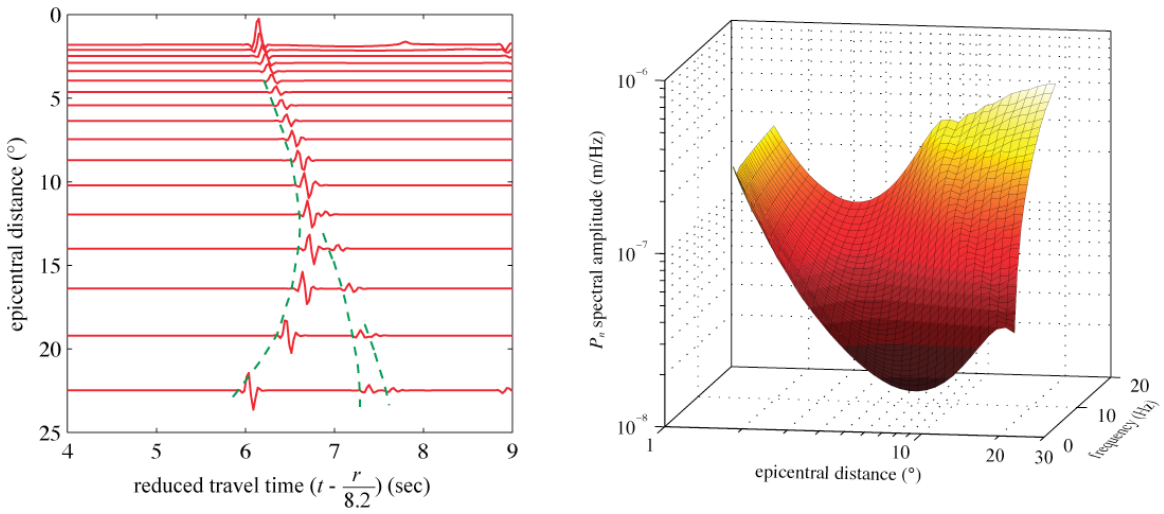

Figure 9. Record section of synthetic Pn seismograms in a spherical Earth model and Pn amplitudes as a function of epicentral distance and frequency. Green lines in the record section mark the first wave pulse (no reflection at Moho), the second wave pulse (one reflection) and the rest of the interference wave packet.

The behavior of Pn geometric spreading in a spherical Earth apparently cannot be accurately represented by a power-law model, which is commonly used. Based on the simulation results, we propose a new, frequency-dependent Pn geometric-spreading model that accounts for the effects of the Earth's sphericity. The new model is formulated as:

$$G(R,f) = \frac{10^{n_3(f)}}{R_0}\left(\frac{R_0}{R}\right)^{n_1(f)\log\left(\frac{R_0}{R}\right)+n_2(f)} \qquad (R_0 = 1 \text{ km}) \quad (1)$$

And

$$n_i(f) = n_{i1}\left[\log\left(\frac{f}{f_0}\right)\right]^2 + n_{i2}\log\left(\frac{f}{f_0}\right) + n_{i3} \qquad (i = 1, 2, 3; f_0 = 1 \text{ Hz}). \quad (2)$$

The main differences between the new geometric-spreading model and the standard frequency-independent power-law model are the addition of the first term in the exponent and the frequency dependence of parameters n_i. In the logarithm domain, the new model is a quadratic function of log-distance, whereas the power-law model is linear. Values of model coefficients n_{ij} obtained by fitting the model to synthetics are listed in Table 1.

Using a set of observed Pn amplitude data from Eurasia, we estimated average Pn attenuation after correcting the amplitudes for geometric spreading with both the new spreading model and power-law models. Results show that the new spreading model yields reasonable Q values, whereas the power-law model results in Q values that are either too large or negative.

Table 1 Coefficients of the new Pn geometric-spreading model

n_{11}	n_{12}	n_{13}	n_{21}	n_{22}	n_{23}	n_{31}	n_{32}	n_{33}
-0.217	1.79	3.16	-1.94	8.43	18.6	-3.39	9.94	20.7

Data Issue For Some 20 SPS BH Asian Seismic Stations

While collecting and measuring amplitudes of Asian seismic events, we have found that some 20 SPS broadband data cannot be reliably measured in the 6 to8 HZ band. This occurs at Project IDA stations AAK, BRVK, KURK, NIL, and TLY. Essentially, at these stations the anti-alias filter begins to roll-off near 5 Hz (Figure 10), and somewhere between 6 and 8 Hz the data stream has been attenuated to below an integer value of one. Thus, velocity spectra of small events flatten near a value of 1, and any attempt to correct these data into displacement artificially boosts the 6 to 8 Hz measurements. When working with displacement amplitudes, this creates a noise floor higher than it should be. Figure 11 shows 20 SPS and 40 SPS displacement amplitudes versus time (in years) from IDA station KURK. For the 4 to 6 Hz measurements, the 20 and 40 SPS instruments are nearly in agreement, but for the 6 to 8 Hz measurements, many of the 20 SPS measurements are high relative to the 40 SPS measurements. This situation does not occur for IC and IU 20 SPS data because the anti-alias roll-off does not begin until 8 Hz (Figure 10, green curve). We recommend that II 20 SPS be measured up to 6 Hz, but not beyond that limit.

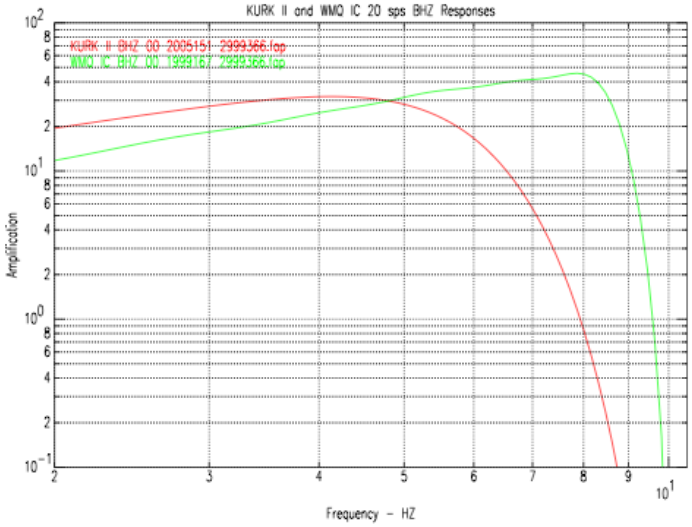

Figure 10. Response curves for 20 SPS II station KURK (in red), and IC station WMQ (in green).

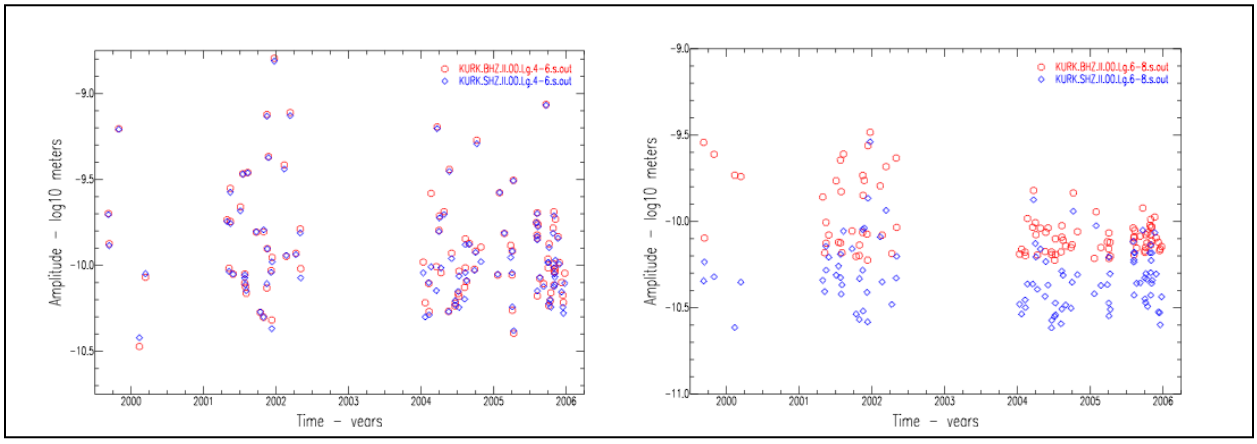

Figure 11. Comparison between KURK II displacement measurements at 20 SPS (red) and 40 SPS (blue) in the 4- 6-Hz (left) and the 6- 8-Hz (right) bands. The 20 SPS 6- 8-Hz measurements are boosted artificially due to early (5 Hz) roll-off of the anti-alias filter. The same situation applies to 20 other SPS II stations in central Asia.

CONCLUSIONS AND RECOMMENDATIONS

We have an ongoing program to identify mining seismicity clusters from waveform correlation and to tie these to overhead imagery for ground truth. For our eastern Kazakhstan study area, we tied 277 out of a total 447 events to 13 distinct mining-event clusters. We have identified features on at least 4 images that clearly show mines within 10 km of our seismic event-cluster locations. By assuming night events are earthquakes, we have been able to test body-wave discriminants. Only the Pg/Lg high-frequency discriminant shows some event separation. The Pg spectral ratio, which does separate earthquakes and nuclear explosions in Asia, does not separate mining explosions from earthquakes in eastern Kazakhstan. We will continue to investigate discriminant measurement and correction methods in an attempt to improve performance in separating mining events from both earthquakes and single-charge underground nuclear events.

In parallel with a project between UCSC and LANL to develop 1-Hz, two-dimensional, regional-phase attenuation models for Eurasia to improve the MDAC discrimination methodology, we are working on developing regional-phase attenuation models for Eurasia for a broad range of frequencies between 0.5 and 10 Hz. We have finished an initial phase of data collection and amplitude measurement for around 100 stations in the region. Based on the data coverage, we collected a dataset of Pn picks from the LANL location database to be used in further data collection. We have also conducted synthetic simulations to investigate the geometric spreading of Pn and Sn in a spherical earth. From the modeling results, we propose new, frequency-dependent Pn and Sn geometric-spreading models for a spherical Earth.

While measuring phase and noise amplitudes using 20 SPS data obtained at IRIS IDA stations operated in Asia, we found that a combination of relatively early anti-alias filter roll-off and operations at relatively low gains, typically results in inaccurate registration of seismic noise and signals (from all but large events) in 6 to 8 Hz bands. Known II stations with this problem include AAK, BRVK, KURK, NIL, and TLY. We recommend measuring amplitudes at frequencies no higher than 6 Hz at these stations and sample rates.

ACKNOWLEDGEMENTS

We thank the entire LANL GNEMRE team for supporting efforts that make this work possible, and we especially thank Richard Stead, Julio Aguilar-Chang, and Diane Baker for their database assembly and maintenance efforts. We thank the IRIS DMC for rapidly filling data requests. We used data from operators and host institutions affiliated with IC, IU, II, KZ, and KN networks. Figure 6 was provided by Cliff Thurber of the University of Wisconsin.

REFERENCES

Červený, V., and R. Ravindra (1971). *Theory of Seismic Head Waves*, University of Toronto Press, Toronto.

Hartse, H. E., S. R. Taylor, W. S. Phillips, and G. E. Randall (1997). A preliminary study of regional seismic discrimination in central Asia with emphasis on western China, *Bull. Seismol. Soc. Am.* 87: 551–568.

Lay, T., X. Yang, X. B. Xie, and M. D. Arrowsmith (2006). Development of regional tomographic attenuation models for Eurasia, in *Proceedings of the 28th Seismic Research Review: Ground-Based Nuclear Explosion Monitoring Technologies,* LA-UR-06-5471, 71-81.

Yang, X. (2002). A numerical investigation of Lg geometrical spreading, *Bull. Seismo. Soc. Am.* 92: 3,067–3,079.